

MIT Open Access Articles

Heat transfer to a horizontal cylinder in a shallow bubble column

The MIT Faculty has made this article openly available. **Please share** how this access benefits you. Your story matters.

Citation: ow, Emily W., and John H. Lienhard V. "Heat Transfer to a Horizontal Cylinder in a Shallow Bubble Column." *International Journal of Heat and Mass Transfer* 79 (December 2014): 353–361.

As Published: <http://dx.doi.org/10.1016/j.ijheatmasstransfer.2014.08.021>

Publisher: Elsevier

Persistent URL: <http://hdl.handle.net/1721.1/102498>

Version: Author's final manuscript: final author's manuscript post peer review, without publisher's formatting or copy editing

Terms of use: Creative Commons Attribution-Noncommercial-Share Alike



Heat transfer to a horizontal cylinder in a shallow bubble column

Emily W. Tow and John H. Lienhard V*

*Rohsenow Kendall Heat Transfer Laboratory
Department of Mechanical Engineering
Massachusetts Institute of Technology
Cambridge, Massachusetts 02139, USA*

Abstract

Heat transfer coefficient correlations for tall bubble columns are unable to predict heat transfer in shallow bubble columns, which have unique geometry and fluid dynamics. In this work, the heat transfer coefficient is measured on the surface of a horizontal cylinder immersed in a shallow air-water bubble column. Superficial velocity, liquid depth, and cylinder height and horizontal position with respect to the sparger orifices are varied. The heat transfer coefficient is found to increase with height until reaching a critical height, and a dimensionless, semi-theoretical correlation is developed that incorporates superficial velocity, liquid properties, and height. Additionally, the more minor effects of flow regime, column region, and bubble impact are discussed with the aim of informing design. Notably, the heat transfer coefficient can be as high in the region of bubble coalescence as in the bulk of the column, but only if the probe is placed so that bubbles impact the cylinder. The correlation and discussion provide a framework for modeling and designing

*Address all correspondence to lienhard@mit.edu

shallow, coil-cooled bubble columns.

Keywords: multiphase flow, turbulent transport, bubble column, sieve tray, dehumidification, heat transfer coefficient

Nomenclature

A	Probe copper area [m ²]
A_c	Probe cross-sectional area [m ²]
C_H	Cylinder height coefficient (Eq. 8) [-]
D	Diameter [m]
H	Vertical position of probe center [m]
L	Length [m]
P	Perimeter [m]
R	Electrical resistance [Ω]
T	Temperature [$^{\circ}\text{C}$]
V	Column volume [m ³]
ΔP	Pressure drop [Pa]
ΔV	Voltage [V]
\dot{E}	Power, input or dissipated [W]
\dot{Q}	Heat transfer rate [W]

\dot{V}	Volume flow rate [m^3/s]
c_p	Specific heat at constant pressure [$\text{J}/\text{kg}\cdot\text{K}$]
d	Column liquid depth [m]
g	Gravitational acceleration [m/s^2]
h	Average heat transfer coefficient [$\text{W}/\text{m}^2\cdot\text{K}$]
k	Thermal conductivity [$\text{W}/\text{m}\cdot\text{K}$]
m	Fin parameter [m^{-1}]
u_g	Superficial gas velocity [m/s]
v_b	Bubble rise velocity [m/s]

Named Ratios

Fr_D	Froude number = $u_g^2/(gD)$ [-]
Nu_L	Nusselt number (of arb. length L) = hL/k [-]
Pr	Prandtl number = $\mu c_p/k$ [-]
Re_D	Reynolds number = $u_g D/\nu$ [-]
St	Stanton number = $h/\rho c_p u_g$ [-]

Greek

ϵ	Specific power dissipation [W/kg]
η	Kolmogorov length scale [m]

μ	Liquid dynamic viscosity [Pa-s]
ν	Liquid kinematic viscosity [m ² /s]
ϕ	Liquid volume fraction [-]
ρ	Liquid density [kg/m ³]
τ	Kolmogorov time scale [s]

Subscripts

∞	Column liquid
<i>ave</i>	Average
<i>C</i>	Column
<i>cr</i>	Critical
<i>end</i>	Probe end caps
<i>p</i>	Probe

1. Introduction

Shallow bubble columns have more intricate fluid dynamics than tall columns as a result of the short distance between the gas sparger and the free surface. Heat transfer to tubing within shallow bubble columns merits further study because of the usefulness of coil-cooled shallow bubble columns in humidification-dehumidification (HDH) desalination [1]. Most bubble column reactors are orders of magnitude taller than those used for dehumidification [2, 3], and therefore the reactor modeling and design literature has

generally focused on the developed (i.e., height-independent) flow region in the middle of the column and neglected to address the entry region near the sparger and the region of bubble coalescence at the free surface. In contrast, a shallow bubble column may have no region of developed flow. Heat transfer coefficients on internal heat exchange elements in sieve tray columns, which are similar in depth to shallow bubble columns, have not been studied because sieve trays have historically been used without such elements. In this work, we investigate heat transfer to cylindrical heat exchange elements in shallow bubble columns.

The results presented herein have applications in the design of shallow bubble column heat and mass exchangers such as bubble column dehumidifiers. The use of sieve tray columns (without coils) for humidification or dehumidification was proposed by Barrett and Dunn in 1974 [4], but more recently, shallow, coil-cooled bubble columns in a multi-tray configuration have proven useful in dehumidification for HDH desalination [1, 5]. In a bubble column dehumidifier, warm, moist air is bubbled through a volume of cool water. The concentration gradient from the warm bubble center to the cool bubble surface drives condensation on the surface of the bubble. The heat leaving the bubbles is then transferred to a cooling coil with a small surface area. Condensation in the presence of high concentrations of noncondensable gases leads to low heat transfer coefficients. However, the key advantage of the bubble column dehumidifier lies in moving the resistive condensation process off an expensive solid surface and onto the surfaces of bubbles.

Bubble columns for dehumidification must be shallow in order to min-

imize the hydrostatic pressure drop and thus the blowing power necessary for dehumidification. In modeling bubble column dehumidification, Tow and Lienhard [3, 6, 7] find the literature lacking studies of heat transfer in shallow bubble columns.

Many geometric parameters affect heat transfer in tall bubble columns with internal heat exchange elements (internals) [8]. Several studies measure the heat transfer coefficient on internals such as cylinders [9, 10, 11, 12, 13] and tube bundles [14] in tall columns. Little is known, however, about the effect of geometry on the heat transfer coefficient in shallow bubble columns with internals. Tow and Lienhard [15] found that cylinder diameter does not significantly affect the heat transfer coefficient outside cylinders in a shallow columns. The influence of additional geometric parameters relevant to shallow columns has not been studied extensively. The heat transfer coefficient has been shown to vary with radial [13] and vertical [16, 13] position in a tall column, and with vertical position in a short column [15]. Narayan et al. [1] proposed that horizontal position of internals with respect to the gas sparger orifices could affect heat transfer coefficients. The heat transfer coefficient in the coalescing region at the top of the column has been shown by Prakash et al. [17] to be significantly lower than in the bulk in an air-water-yeast system, but this has not been studied in an air-water system. Finally, to our knowledge, the effect of liquid depth on heat transfer coefficient or flow regime has not been studied.

In this paper, the heat transfer coefficient for a horizontal cylinder in a shallow (<10 cm deep) air-water bubble column is measured over a range of gas superficial velocities. Liquid depth, cylinder height, and cylinder hori-

zontal position relative to the sparger orifices are varied in order to determine the effect of height, column region, flow regime and bubble impact (bubbles directly hitting the coil) on the heat transfer coefficient. Of the variables considered, probe height proves to have the most profound effect on heat transfer coefficient. Therefore, a semi-theoretical correlation for the heat transfer coefficient in shallow bubble columns is developed in the form of a height correction factor applied to Deckwer's [18] theory for tall bubble columns. Finally, the minor effects of column region, flow regime and bubble impact that are excluded from the correlation are discussed qualitatively to inform shallow bubble column design.

1.1. Theoretical Background

Many correlations predict the heat transfer coefficient in bubble columns, but there is significant disagreement between them in terms of heat transfer coefficient magnitude, superficial velocity dependence, and included geometric variables. Several reviews of bubble column heat transfer coefficient correlations are available [2, 8, 12, 19, 20, 21], and the spread in the predictions is demonstrated by a comparison of ten correlations by Hikita et al. [22]. Most correlations are semi-theoretical with forms that depend on the assumed mode of heat transfer. Many correlations assume heat is transported by microscale eddies produced by the dissipation of bubbles' flow work. Others consider fluid elements with a different length scale, such as the bubble diameter or distance between bubbles. Other disparities may be due to differences in measurement methods and, particularly in the case of correlations for internals, geometry.

We have found no correlation developed for tall columns that satisfacto-

rily predicts the heat transfer coefficient in a shallow column, but we have demonstrated agreement with several correlations with respect to the dependence on superficial velocity [15]. One of these correlations is Deckwer’s [18], which is straightforward and widely-used. This semi-theoretical correlation is based on the dissipation of bubbles’ flow work by small (Kolmogorov scale) eddies which interact periodically with the heat transfer surface. Turbulence is assumed to be isotropic and uniform throughout the column. The thermal interactions between eddies and the solid surface are modeled as conduction through a semi-infinite slab with a characteristic time equal to the Kolmogorov time scale, $\tau = \sqrt{\nu/u_g g}$. The application of an empirical constant leads to the correlation, Eq. 1 [18]:

$$\text{St} = 0.1(\text{Re}_D \text{Fr}_D \text{Pr}^2)^{-1/4} \quad (1)$$

To rewrite Eq. 1 in a simpler form, we consider a bubble column with volume V , liquid density ρ , and liquid fraction ϕ . Assuming high density ratio between liquid and gas, the total energy dissipation rate \dot{E} is the product of specific dissipation rate ϵ and liquid mass:

$$\dot{E} = \epsilon V \rho \phi. \quad (2)$$

The power input is determined by the volume flow rate of bubbles and the hydrostatic pressure drop through the column. Bubbles flow in at volume flow rate \dot{V} against the pressure drop $\Delta P = \rho \phi g d$, where d is the liquid depth. The column cross-sectional area is V/d . The power input is then:

$$\dot{E} = \dot{V} \Delta P = u_g (V/d) \rho \phi g d = u_g V \rho \phi g, \quad (3)$$

where u_g is the superficial gas velocity.

In steady state, the power input is equal to the power dissipated. Setting Eqs. 2 and 3 equal, we find (as did Deckwer [18]):

$$\epsilon = u_g g. \quad (4)$$

The Kolmogorov length scale $\eta = (\nu^3/\epsilon)^{1/4}$ in a bubble column is therefore given by Eq. 5:

$$\eta = \left(\frac{\nu^3}{u_g g}\right)^{1/4}. \quad (5)$$

Using Eq. 5, Deckwer's correlation can then be rearranged [3] as Eq. 6, a Nusselt number correlation based on the Kolmogorov length for a bubble column:

$$\text{Nu}_\eta = 0.1\text{Pr}^{1/2}. \quad (6)$$

The present authors believe that this representation better illustrates that heat transfer is accomplished by transient thermal interactions with microscale eddies. Although the dependence on $\text{Pr}^{1/2}$ may seem unusual, it is not unique to this correlation. For example, Hughes and Duffey [23] propose a theoretical correlation for direct contact condensation in a turbulent flow (in which η is defined generally as $\eta = [\nu^3/\epsilon]^{1/4}$) that can be stated in the same form:

$$\text{Nu}_\eta = \frac{2}{\sqrt{\pi}}\text{Pr}^{1/2}. \quad (7)$$

In both cases the form of the correlation results from modeling heat transfer with Higbie's surface renewal theory [24] and evaluating the interaction period as the Kolmogorov time scale. However, Deckwer's correlation acknowledges with an application-specific empirical constant that η is more of a scaling than an exact length.

Deckwer’s correlation was shown by Deckwer et al. [25] to successfully predict heat transfer coefficients in hydrocarbon liquids with Prandtl numbers as high as 225 (Paraffin at 143°C), and reported by Shah et al. [26] to be valid within $6 < \text{Pr} < 985$.

Joshi et al. [27] propose another correlation (Eq. 8) for the heat transfer coefficient in a tall column based on an analogy with stirred tanks.

$$\text{Nu}_{D_C} = 0.48 \left(\frac{\rho D_C^{4/3} g^{1/3} [u_g - (1 - \phi)v_b]}{\mu} \right)^{2/3} \text{Pr}^{1/3} \left(\frac{\mu}{\mu_p} \right)^{1/3} \quad (8)$$

Unlike Deckwer’s correlation, the heat transfer coefficient of Eq. 8 varies with column diameter and includes a correction to account for the viscosity variation between the heated surface (μ_p) and the bulk (μ). Despite this, Shah et al. [26] find in their review that both correlations work equally well and conclude that these approaches “can be regarded as limiting cases of a more general model.”

We have previously shown that the heat transfer coefficient in a shallow column depends on the distance, H , from the sparger plate [15], and we wish to quantify this effect with a correlation that utilizes the vast amount of existing knowledge about heat transfer in tall bubble columns. Of the two correlations mentioned, Deckwer’s is more straightforward. Therefore, we propose a modification to Deckwer’s correlation of the following form:

$$\text{Nu}_\eta = C_H \text{Pr}^{1/2}, \quad (9)$$

where C_H is an unknown function of height. A correlation of this form makes it possible to account for the deviation from uniform turbulence near the solid sparger. In Sec. 3.3, experimental measurements are used to evaluate C_H for the shallow column used in this work.

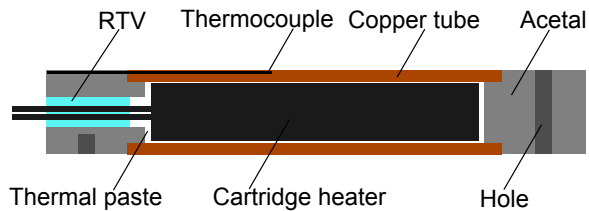


Figure 1: Schematic diagram of the heat transfer coefficient probe construction

2. Experimental Methods

The heat transfer coefficient outside a horizontal cylinder in a shallow bubble column is measured using a cylindrical heat transfer coefficient probe. A cylindrical probe is used to represent coils of large turn radius compared to the outer diameter of the tube, for which the effects of coil curvature would be negligible. Gas superficial velocity, probe diameter, liquid height, probe height, and horizontal cylinder position with respect to the sparger holes are varied. Additionally, the flow regime is observed for a range of liquid depths and gas velocities.

2.1. Heat Transfer Coefficient Probe Design

The heat transfer coefficient probe, which consists of a cartridge heater inside a copper tube instrumented with several thermocouples (Fig. 1), dissipates a known power over a known area and measures the surface temperature. A separate thermocouple measures the bubble column bulk temperature, T_∞ . The probe ends are sealed and insulated with acetal caps ($k_{acetal} = 0.33 \text{ W/m-K}$ [28]). As described by Tow and Lienhard [15], the average heat transfer coefficient can be calculated using Eq. 10,

$$h = \frac{\dot{Q}_p - 2\dot{Q}_{end}}{A(T_{p,ave} - T_\infty)}, \quad (10)$$

where A is the surface area of the probe's copper tube, T_∞ is the column bulk temperature, the power dissipated is:

$$\dot{Q}_p = \frac{\Delta V^2}{R}, \quad (11)$$

and where the minimal ($\sim 1\%$) heat loss at each end is approximately:

$$\dot{Q}_{end} \approx \sqrt{hP_p k_{acetal} A_c} (T_{end,ave} - T_\infty). \quad (12)$$

$T_{end,ave}$ is the average reading of the two thermocouples closest to the end caps. The infinitely-long fin approximation of Eq. 12 can be applied to the end caps because the fin is much longer than its extinction length (m_{end}^{-1}), as shown by Eq. 13:

$$(mL)_{end} = \sqrt{\frac{hP_p}{k_{acetal} A_c}} L_{end} \approx 18 \text{ to } 120 \gg 1. \quad (13)$$

The effect of the diameter of cylindrical internals has been investigated by several authors, but there is disagreement among them [8, 29, 10, 30]. Among the three probes tested by Tow and Lienhard [15] (4.76, 9.53, and 15.88 mm in diameter), no significant effect of probe diameter on heat transfer coefficient was observed. Therefore, all measurements in the present study are made with a single probe, 9.53 mm (3/8") in diameter.

The construction of the probe is detailed in [15] and [31] and summarized here. The probe has a 62.2 mm-long heated copper test section and 25.4 mm-long press-fit acetal end caps. Four thermocouples are distributed in a spiral, covering the probe evenly in both axial and radial directions; the

four readings are averaged to represent the average surface temperature. The thermocouples are 36-gauge K-type with fiberglass insulation. The thermocouple attachment method is detailed in [31].

Tow and Lienhard [15] validated the probe against the correlation of Churchill and Chu [32] for natural convection from a horizontal cylinder, and found that the 9.53 mm probe used here measured heat transfer coefficients within 8% of the predicted value. The probe is designed to have a 95% confidence interval of $\pm 12.4\%$ of the heat transfer coefficient measurement [31]. This uncertainty accounts for the 1.1°C uncertainty on each individual thermocouple (except for the thermocouple measuring the bath temperature, which was calibrated to reduce its uncertainty). Additional uncertainty of around 3% [31] arises from calculating the average temperature of the probe surface with only four measurements. The uncertainty in the measurement could not be lowered by operating at a larger temperature difference because a low temperature difference is required between the probe and the water to minimize the formation of air bubbles on the probe surface.

2.2. Experimental Apparatus

The heat transfer coefficient probes fit into an experimental fixture in which the gas velocity, liquid depth, sparger design, and cylinder diameter, height, and horizontal position relative to the sparger orifices can be easily varied. Figure 2 shows the experimental setup.

The bubble column is contained by a rectangular polycarbonate tank, 157 mm wide and 284 mm long, that can be filled to a maximum depth of 110 mm above the sparger plate. The tank width can be considered to be large based on observations about tall bubble columns: at this hydraulic diameter

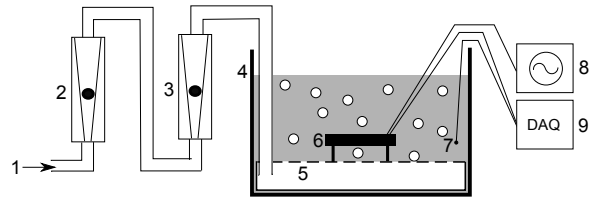


Figure 2: Experimental apparatus: 1. Pressurized dry air inlet; 2. Rotameter (4-40 cfm); 3. Rotameter (0.4-4 cfm); 4. Tank; 5. Orifice plate sparger; 6. Heat transfer coefficient probe; 7. Thermocouple; 8. Variable autotransformer; 9. Data acquisition unit.

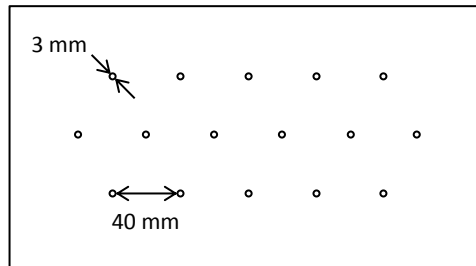


Figure 3: Sparger plate used in experimental column

(202 mm), the gas holdup is independent of column diameter [2] and the heat transfer coefficient is within 10% of the large-diameter value [8]. The sparger plate, depicted in Fig. 3, has sixteen 3 mm orifices spaced 40 mm apart in a triangular grid.

2.3. Experimental Protocol

First, tap water is degassed by boiling and cooling. The probe is polished to remove oxidation and installed in the desired position. In the case of bubble impact, the probe is placed over the central row of sparger orifices, and otherwise it is placed between rows. The column is filled with degassed water to the desired depth during air sparging at 1 cm/s. A wide ruler is

positioned a few millimeters from the front wall of the tank to damp the liquid depth fluctuations in the vicinity of the depth measurement without causing significant capillary rise. The heater and DAQ are turned on, and the heater voltage is measured. Ice and/or hot degassed water are added until the column reaches 20°C. The system is allowed a few minutes to reach a quasi-steady state in which there is a constant temperature difference between the probe surface and column liquid.

To make each measurement, the air flow rate is set and the system is given about one minute to return to a quasi-steady state. Air bubbles that accumulate on the warm probe due to the outgassing of air from the water (which, despite initial degassing efforts, tends to reabsorb air during bubbling) are brushed off with a curved pipe cleaner. Because of this bubble-removal procedure, these measurements apply to heat transfer coefficients in cooling, which is the direction of heat transfer in dehumidification and many chemical processing applications, including Fischer-Tropsch synthesis [33]. Finally, approximately sixty measurements of each temperature are taken with the DAQ at half-second intervals. The average temperature of each thermocouple is recorded for use in computing the heat transfer coefficient. This procedure is repeated for a number of air flow rates for each column-probe configuration.

Throughout the experiment, bulk liquid temperature is maintained as close as possible to 20°C. The film temperature (the average temperature of the bulk liquid and probe surface) was $23.8^{\circ}\text{C} \pm 1.0^{\circ}\text{C}$, indicating that the liquid properties (particularly viscosity) can be considered constant across all measurements.

3. Correlation Development

Superficial velocity, liquid depth, probe height, and horizontal probe position with respect to the sparger holes were varied to determine the effects of geometry on the heat transfer coefficient. Of the variables tested, probe height has the most dramatic effect on heat transfer coefficient, and therefore only height is incorporated into the correction to Deckwer’s correlation [18]. The effects of liquid depth and horizontal probe position, which determine the flow regime, column region, and incidence of bubble impact, are discussed further in Sec. 4. In this section, the experimental results for cylinder height are presented, a dimensionless height ratio is justified, and a correlation is developed.

3.1. *Effect of Probe Height*

To understand the effect of cylinder height, it is first necessary to understand the regions of fluid flow in the column. As in tall bubble columns and sieve trays, the flow pattern in shallow columns varies in the vertical direction. For the range of superficial velocities tested here, the top 2 cm or so of fluid has a high void fraction. As described by Joshi and Shah [34] for tall bubble columns, this region is where bubbles pile up, coalesce, and join the continuous gas phase above the column. Therefore, this region will be referred to as the “coalescing” region. Below the coalescing region, the void fraction is high. Despite the height-dependent flow that would be considered to be “developing” in a tall column, everything below the coalescing region will be referred to herein as the “bulk.” In this work, “coalescing” measurements were always made with the probe even with the top surface

of the liquid so that the top of the probe was just kept wet, and “bulk” measurements were made at least 2 cm beneath the surface.

In shallow bubble columns, the heat transfer coefficient depends on the height at which the cylinder is placed. Far from the sparger plate, the flow of heat-carrying eddies is unaffected by the plate and the heat transfer coefficient is roughly independent of height. However, below the critical modified Reynolds number, the presence of the solid plate hinders the heat transport. The effect of cylinder height on heat transfer coefficient is shown in Figs. 4 and 5 for the bulk and coalescing regions, respectively. In each figure, the liquid depth and cylinder height (the vertical position of the probe center with respect to the sparger) are varied together. In the coalescing region measurements, the liquid is just deep enough to keep the probe wet. In the bulk region measurement, the free surface is maintained 2 cm above the top of the probe.

The heat transfer coefficient increases monotonically with height until reaching a maximum¹ at 4.5 cm in both regions. Similar heat transfer coefficients are measured at a height of 8.5 cm. The significant drop in heat transfer coefficient as the probe height is reduced from 4.5 to 0.5 cm is unsurprising because the bottom wall (the sparger) acts as a momentum sink, decreasing the turbulent dissipation rate in its vicinity. Prakash et al. [17] similarly observe that the heat transfer coefficient in a tall bubble column decreases in the vicinity of the column wall.

¹The peak in heat transfer coefficient around a height of 4.5 cm observed in the experimental column is most likely due to the height-dependent bubble dynamics that have been observed by several researchers [35, 34, 31] in the developing region near the sparger.

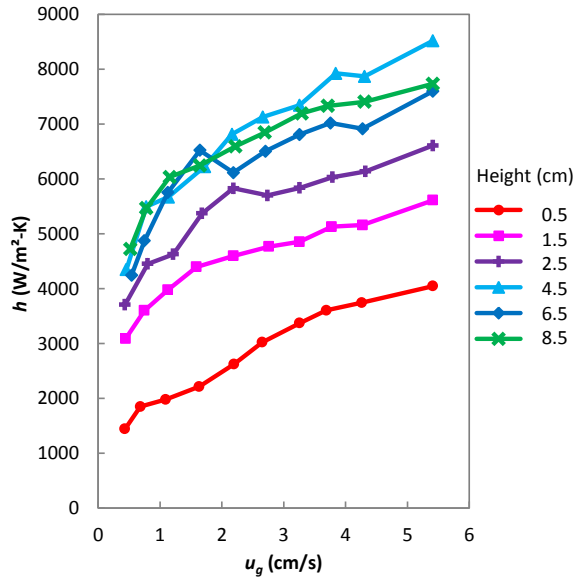


Figure 4: Heat transfer coefficients in the bulk region with impact at a variety of heights (data from Tow and Lienhard [15]). The fluid is depth maintained at 2 cm over the top of the probe except (3 cm in the case of the 6.5 cm-high probe).

The data show a critical height (around 3 cm in this experiment) above which the heat transfer coefficient is roughly constant and below which the heat transfer coefficient varies with cylinder height above the sparger. A more general critical height is discussed in Sec. 3.4.

3.2. Dimensionless Height Ratio

The critical height below which heat transfer is influenced by the presence of the sparger plate can be understood through an analogy to fluid dynamics. Above a certain depth, the liquid has bulk motion (swirling or sloshing, discussed further in the appendix), but below a this depth, the proximity of the sparger plate prevents bulk motion and only splashing is observed.

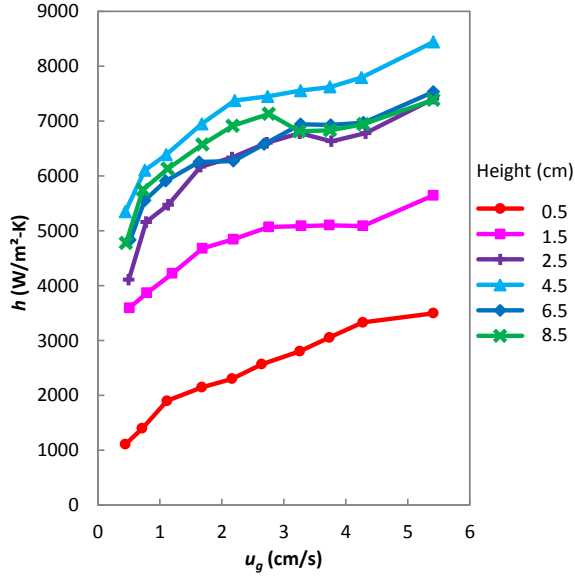


Figure 5: Heat transfer coefficients in the coalescing region with impact at a variety of probe heights

The transition from splashing to sloshing flow can be measured over a range of superficial velocities by varying the liquid depth. As shown in Fig. 6, the transition between flow regimes occurs at a height of 900η , where η is the Kolmogorov length scale, Eq. 5. The constant d/η ratio marking the transition to sloshing suggests that η could nondimensionalize the height as it relates to heat transfer as well. Therefore, we adopt h/η as a dimensionless height ratio.

The experiments used in the correlation of Sec. 3.3 span only a small range of η (34-66 μm), and the cross-section of the column was not varied, so it is possible that h/η is not the only relevant dimensionless height. Further experimentation is necessary to hone in on a universal correlation.

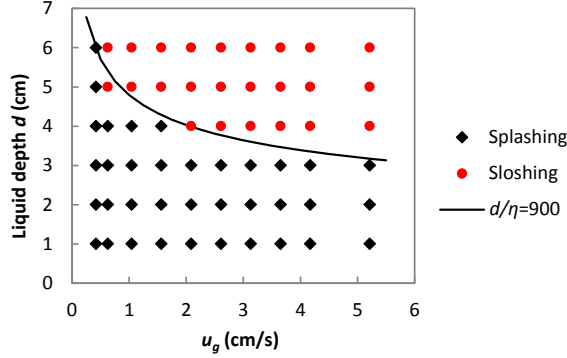


Figure 6: Observation suggests that the liquid depth at the onset of sloshing is related to the ratio d/η

3.3. Correlation

Due to the strong variation in heat transfer coefficient with probe height shown by Figs. 4 and 5, we develop a correlation incorporating probe height as well as the superficial velocity and liquid properties captured by existing tall column correlations. Experimental data from Figs. 4, 5, 9, and 10 along with data from Tow and Lienhard [15, 31] using the same test column with two additional probes (of diameters 4.76 and 15.88 mm and with 11-14% measurement uncertainty in h) are utilized to find the coefficients of a semi-theoretical correlation of the form proposed in Eq. 9. It is assumed that C_H is a function of the dimensionless height ratio, H/η , as argued in Sec. 3.2.

To find a correlation of the form: $\text{Nu}_\eta = C_H(H/\eta)\text{Pr}^{1/2}$, we compare the measured value of $\text{Nu}_\eta/\text{Pr}^{1/2}$ to H/η as shown in Fig. 7. The approach of $\text{Nu}_\eta/\text{Pr}^{1/2}$ to a constant value can be described by an exponential function, Eq. 14, with three unknown coefficients:

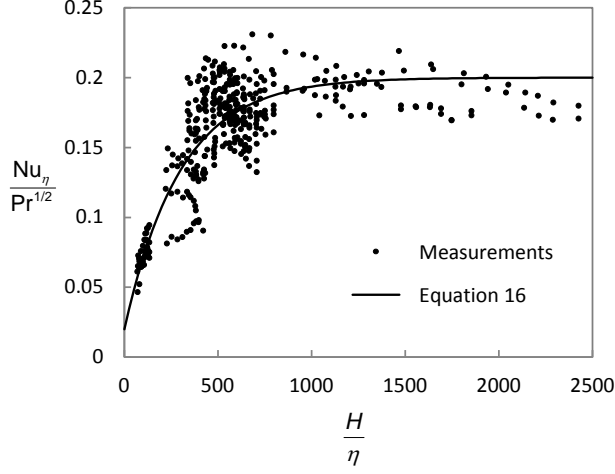


Figure 7: Correlation of C_H with the ratio h/η

$$C_H = a + b \left[1 - \exp \left(\frac{-H}{c\eta} \right) \right]. \quad (14)$$

Coefficients a , b , and c were varied until the average absolute error between the correlation and the 389 measurements was minimized to within 0.1%. The resulting correlation is given by Eqs. 15 and 16:

$$\text{Nu}_\eta = C_H \text{Pr}^{1/2}, \quad (15)$$

where

$$C_H = 0.02 + 0.18 \left[1 - \exp \left(\frac{-H}{300\eta} \right) \right], \quad (16)$$

and where η is the Kolmogorov length scale, Eq. 5. The correlation is compared with the data in Fig. 8. The correlation and data agree with an average absolute error of 10.8%, and 85% of the measurements fall within 20% of the correlation.

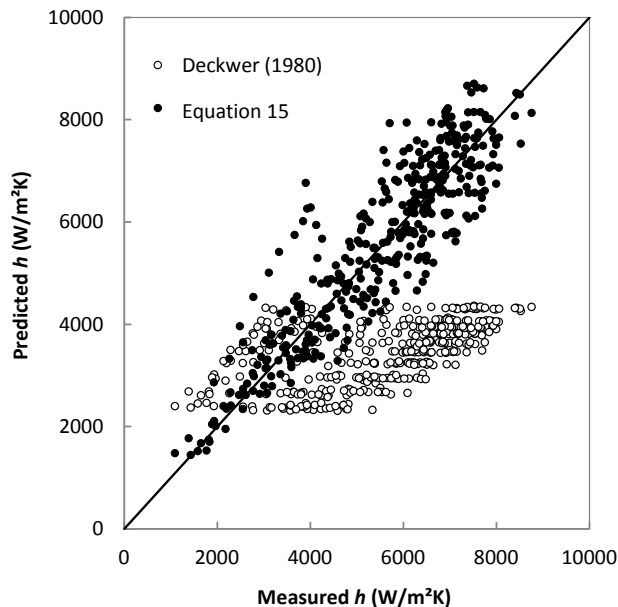


Figure 8: Agreement of Eq. 15 with shallow column experimental data from this work and from Tow and Lienhard [15, 31]. Predictions from Deckwer’s correlation for tall columns [18] are also shown for comparison.

Figure 8 also includes a comparison to Deckwer’s popular correlation for tall columns [18] (Eq. 1), which shows that while Deckwer’s correlation predicts shallow column heat transfer coefficients of the correct order or magnitude, Eq. 15 improves the accuracy by capturing the important effect of height.

Some spread still exists because Eq. 15 incorporates only the effect of probe height, whereas the more minor effects of flow regime, column region, and bubble impact are excluded from the correlation. The magnitudes of these effects may be specific to the column and sparger design, but the trends are likely to be more general. For this reason, the trends associated with these

factors are discussed in Sec. 4.

This correlation has not been tested in columns of differing cross-section or with different liquids, and should be applied with caution. However, the observed decline in heat transfer coefficient as the heat exchange element approaches the sparger plate should be expected in a wide range of column designs.

3.4. Critical Height

Above a critical height, the effect of the sparger plate on the heat transfer coefficient is negligible and a simpler correlation, $\text{Nu}_\eta = 0.2\text{Pr}^{1/2}$, can be used. Based on the form the height-dependent correction factor, Eq. 16, the critical height (at which the heat transfer coefficient is 90% of its value very far from the sparger) is $H_{cr} = 660\eta$.

Under conditions typical of this experiment (3 cm/s superficial velocity and 23°C water), the predicted critical height is 2.7 cm, which is consistent with the transition to height-independent heat transfer coefficient between the heights of 2.5 and 4.5 cm shown in Figs. 4 and 5.

4. Observations

Despite being excluded from the correlation, the minor effects of flow regime, column region, and bubble impact are nonetheless useful to consider when designing a shallow bubble column. The effects of these three variables are discussed qualitatively in this section. Although the exact results are specific to the test column, the trends are likely to be general.

4.1. Flow Regime

The heat transfer coefficient depends weakly on the flow regime as shown in Fig. 9. The flow regimes (splashing, sloshing, or swirling), described in the appendix, vary with superficial velocity and liquid depth. The heat transfer coefficient is slightly higher in swirling than in sloshing flow. The highest and lowest heat transfer coefficients are measured in splashing, with and without impact, respectively. However, because splashing requires a shallow liquid (see appendix), it is impossible to place a probe in the bulk of a splashing liquid without bringing it very close to the sparger. Therefore, the measurements of the splashing regime are taken in the coalescing region, which is discussed in Sec. 4.2, and consequently the splashing regime cannot be compared directly to the other regimes in the bulk region. However, for a fixed probe height (as in Fig. 9), changing the liquid depth does change the flow regime and, to a lesser extent, the heat transfer coefficient. Because the effect of flow regime on heat transfer is not very pronounced, the depth of the column can be chosen based on other constraints such as blowing power.

4.2. Column Region and Bubble Impact

We find that the column region occupied by the internals matters somewhat, depending on the incidence of bubble impact. Therefore, column region and bubble impact are discussed together in this section. The distinction between coalescing and bulk regions was discussed in Sec. 3.1.

When heat transfer in different regions of an air-water-yeast bubble column were measured, the heat transfer coefficient in the bulk was more than twice that in the coalescing region [17]. The surface-active properties of yeasts [36] (absent in this experiment) stabilize the air-water-yeast foam and

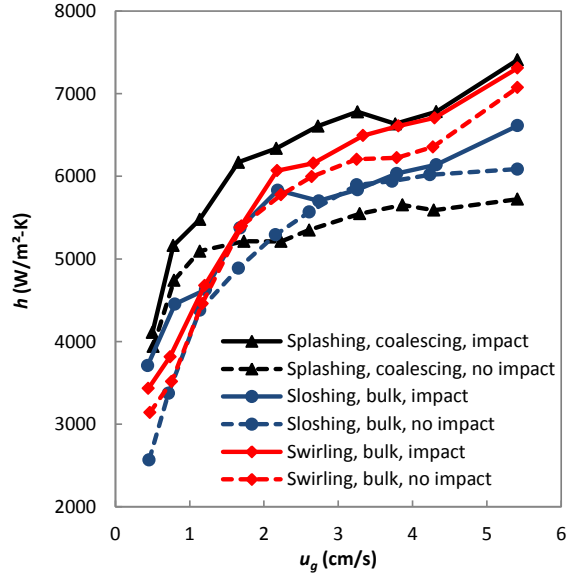


Figure 9: Heat transfer coefficient variations with changes in flow regime. For these measurements, the probe height was fixed at 2.5 cm and the liquid depth was varied (2.5, 5, and 10 cm for splashing, sloshing, and swirling, respectively).

reduce turbulence in that region. In contrast, the air-water foam in the present experiment is not stabilized by surfactants, leading to a violent coalescing region. Figure 10 shows that, particularly in the case of impact, the heat transfer coefficients in the coalescing region are comparable to those in the bulk region. This can also be seen by comparison of Figs. 4 and 5, which show heat transfer coefficients in the bulk and coalescing regions, respectively.

Bubble impact, proposed as a variable of interest by Narayan et al. [1], was also tested because of observations by Tow and Lienhard [3] that aligning a cooling coil directly above sparger orifices led to a consistently (albeit slightly) higher effectiveness in a shallow bubble column dehumidifier. The ef-

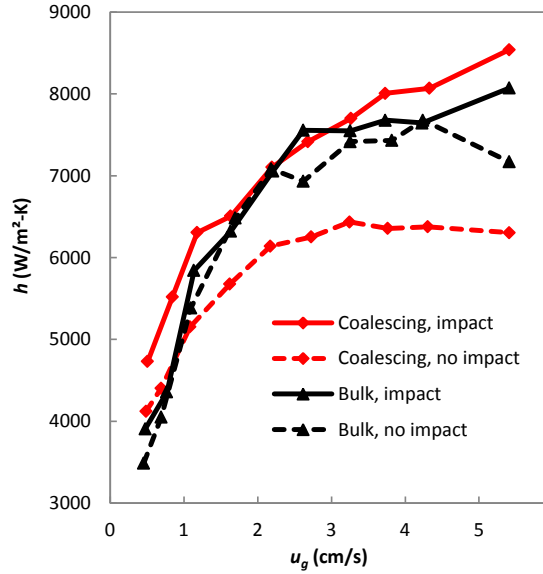


Figure 10: The heat transfer coefficient in the bulk of the fluid and in the coalescing region, with and without impact. In each case the probe height was 2.5 cm; the region was changed by varying the liquid depth (2.5 and 10 cm for coalescing and bulk, respectively).

fect of bubble impact on heat transfer coefficient was measured in the present work by varying the horizontal position of the probe with respect to the rows of sparger orifices. In the case of impact, the probe was positioned over the central two orifices in Fig. 3, and in the non-impact case it was positioned between the central and front rows of orifices. Figure 10 shows that although impact does not matter in the bulk, it clearly affects heat transfer in the coalescing region.

This variation in impact-dependence makes it clear that the mode of heat transfer in the coalescing regime is different. Due to the locally high void fraction, the uniform turbulence assumption may not be valid in the coalescing region. In addition, contact with liquid filaments and droplets

created by the bursting of bubbles may enhance heat transfer in the impact case.

The highest heat transfer coefficients occur in the coalescing region with impact, and nearly as high were measurements in the bulk regardless of impact. In the case of no impact, the coalescing region proves to perform worse than the bulk. Clearly, the correlation is unable to predict the heat transfer coefficient in the coalescing regime without impact. However, we now know that good shallow column design will steer clear of this configuration. Because high heat transfer coefficients extend into the coalescing region in the presence of impact, blowing power can be reduced by setting the liquid depth so that the coil is just covered.

5. Conclusions

Measurements of the heat transfer coefficient on a cylinder in a shallow bubble column demonstrate how geometric parameters influence heat transfer in shallow bubble columns:

- Heat transfer coefficients increase with cylinder height until reaching a critical height
- Above the critical height, the highest heat transfer coefficients occur when the cylinder is in the coalescing region and aligned over the sparger holes
- Compared to the effect of cylinder height, the effects of flow regime, column region, and bubble impact on heat transfer are minimal.

Based on these observations, a semi-theoretical correlation (Eq. 15) is developed that predicts the heat transfer coefficients on a cylinder in a shallow bubble column as a function of cylinder height, superficial velocity, and liquid properties. The more minor effects on heat transfer coefficient are discussed to provide insight into effective shallow bubble column design.

6. Acknowledgment

We would like to acknowledge support from the King Fahd University of Petroleum and Minerals through the Center for Clean Water and Clean Energy at MIT and KFUPM (Project #R4-CW-08). We would like to thank Immanuel David Madukauwa-David for taking preliminary measurements and refining the experimental protocol. The first author would like to acknowledge support from the Flowers Family Fellowship and the Pappalardo Fellowship. This material is based upon work supported by the National Science Foundation Graduate Research Fellowship Program under Grant No. 1122374.

References

- [1] G. P. Narayan, M. H. Sharqawy, S. Lam, S. K. Das, J. H. Lienhard V, Bubble columns for condensation at high concentrations of noncondensable gas: Heat-transfer model and experiments, *AIChE Journal* 59 (2013) 1780–1790.
- [2] N. Kantarci, F. Borak, K. O. Ulgen, Review: Bubble column reactors, *Process Biochemistry* 40 (2005) 2263–2283.

- [3] E. W. Tow, J. H. Lienhard V, Experiments and modeling of bubble column dehumidifier performance, *International Journal of Thermal Sciences* 80 (2014) 65–75.
- [4] E. C. Barrett, S. G. Dunn, Design of direct contact humidifiers and dehumidifiers using tray columns, *Industrial & Engineering Chemistry Process Design and Development* 13 (1974) 353–358.
- [5] K. M. Chehayeb, F. K. Cheaib, J. H. Lienhard V, A heat and mass transfer model of a desalination system based on packed-bed humidification and bubble column dehumidification, in: *Proceedings of the 15th International Heat Transfer Conference, Kyoto, Japan, August 10-15, 2014 (accepted)*. Paper #IHTC15-8995.
- [6] E. W. Tow, J. H. Lienhard V, Analytical modeling of a bubble column dehumidifier, in: *Proceedings of the ASME Summer Heat Transfer Conference, Vol. 3, Minneapolis, MN, July 14-19, 2013*. Paper #HT2013-17763.
- [7] E. W. Tow, J. H. Lienhard V, Heat flux and effectiveness in bubble column dehumidifiers for HDH desalination, in: *Proceedings of the International Desalination Association World Congress on Desalination and Water Reuse, Tianjin, China, Oct 20-25, 2013*. Paper #TIAN13-121.
- [8] A. K. Jhawar, A. Prakash, Heat transfer in a slurry bubble column reactor: A critical overview, *Industrial & Engineering Chemistry Research* 51 (2012) 1464–1473.

- [9] S. C. Saxena, R. Vadivel, A. C. Saxena, Gas holdup and heat transfer from immersed surface in two- and three-phase systems in bubble columns, *Chemical Engineering Communications* 85 (1989) 63–83.
- [10] S. C. Saxena, B. B. Patel, Heat transfer investigations in a bubble column with immersed probes of different diameters, *International Communications in Heat and Mass Transfer* 18 (1991) 467 – 478.
- [11] M. Nishikawa, H. Kato, K. Hashimoto, Heat transfer in aerated tower filled with non-newtonian liquid, *Industrial & Engineering Chemistry Process Design and Development* 16 (1977) 133–137.
- [12] M. O. O. Kagumba, Heat transfer and bubble dynamics in slurry bubble columns with internals for Fischer-Tropsch synthesis of clean alternative fuels and chemicals, Ph.D. thesis, Missouri University of Science and Technology, 2013.
- [13] H. Li, A. Prakash, Survey of heat transfer mechanisms in a slurry bubble column, *The Canadian Journal of Chemical Engineering* 79 (2001) 717–725.
- [14] H. Korte, Heat transfer in bubble columns with and without internals, Ph.D. thesis, University of Dortmund, 1987.
- [15] E. W. Tow, J. H. Lienhard V, Measurements of heat transfer coefficients to cylinders in shallow bubble columns, in: *Proceedings of the 15th International Heat Transfer Conference, Kyoto, Japan, August 10-15, 2014 (accepted)*. Paper #IHTC15-8857.

- [16] S. C. Saxena, N. S. Rao, A. C. Saxena, Heat transfer and gas holdup studies in a bubble column: Air-water-sand system, *The Canadian Journal of Chemical Engineering* 70 (1992) 33–41.
- [17] A. Prakash, A. Margaritis, H. Li, M. A. Bergougnou, Hydrodynamics and local heat transfer measurements in a bubble column with suspension of yeast, *Biochemical Engineering Journal* 9 (2001) 155 – 163.
- [18] W.-D. Deckwer, On the mechanism of heat transfer in bubble column reactors, *Chemical Engineering Science* 35 (1980) 1341 – 1346.
- [19] C. Hulet, P. Clement, P. Tochon, D. Schweich, N. Dromard, J. Anfray, Literature review on heat transfer in two- and three-phase bubble columns, *International Journal of Chemical Reactor Engineering* 7 (2009).
- [20] S. C. Saxena, N. S. Rao, Heat transfer and gas holdup in a two-phase bubble column: Air-water system – review and new data, *Experimental Thermal and Fluid Science* 4 (1991) 139 – 151.
- [21] S. Schluter, A. Steiff, P.-M. Weinspach, Heat transfer in two- and three-phase bubble column reactors with internals, *Chemical Engineering and Processing: Process Intensification* 34 (1995) 157 – 172.
- [22] H. Hikita, S. Asai, H. Kikukawa, T. Zaike, M. Ohue, Heat transfer coefficient in bubble columns, *Industrial & Engineering Chemistry Process Design and Development* 20 (1981) 540–545.

- [23] E. D. Hughes, R. B. Duffey, Direct contact condensation and momentum transfer in turbulent separated flows, *International Journal of Multiphase Flow* 17 (1991) 599 – 619.
- [24] R. Higbie, The rate of absorption of a pure gas into a still liquid during short periods of exposure, *AIChE Journal* 31 (1935) 365–389.
- [25] W.-D. Deckwer, Y. Louisi, A. Zaidi, M. Ralek, Hydrodynamic properties of the fischer-tropsch slurry process, *Industrial & Engineering Chemistry Process Design and Development* 19 (1980) 699–708.
- [26] Y. T. Shah, B. G. Kelkar, S. P. Godbole, W.-D. Deckwer, Design parameters estimations for bubble column reactors, *AIChE Journal* 28 (1982) 353–379.
- [27] J. B. Joshi, M. M. Sharma, Y. T. Shah, C. P. P. Singh, M. Ally, G. E. Klinzing, Heat transfer in multiphase contactors, *Chemical Engineering Communications* 6 (1980) 257–271.
- [28] P. Samyn, P. D. Baets, Friction and wear of acetal: A matter of scale, *Wear* 259 (2005) 697 – 702.
- [29] V. V. Konsetov, Heat transfer during bubbling of gas through liquid, *International Journal of Heat and Mass Transfer* 9 (1966) 1103 – 1108.
- [30] K. Muroyama, S. Okumichi, Y. Goto, Y. Yamamoto, S. Saito, Heat transfer from immersed vertical cylinders in gas-liquid and gas-liquid-solid fluidized beds, *Chemical Engineering & Technology* 24 (2001) 835–842.

- [31] E. W. Tow, Heat and Mass Transfer in Bubble Column Dehumidifiers for HDH Desalination, Master's thesis, Massachusetts Institute of Technology, 2014. doi: <http://hdl.handle.net/1721.1/87970>.
- [32] S. W. Churchill, H. H. Chu, Correlating equations for laminar and turbulent free convection from a horizontal cylinder, *International Journal of Heat and Mass Transfer* 18 (1975) 1049 – 1053.
- [33] C. Maretto, R. Krishna, Modelling of a bubble column slurry reactor for fischer-tropsch synthesis, *Catalysis Today* 52 (1999) 279 – 289.
- [34] J. B. Joshi, Y. T. Shah, Invited review: Hydrodynamic and mixing models for bubble column reactors, *Chemical Engineering Communications* 11 (1981) 165–199.
- [35] I. Leibson, E. Holcomb, A. G. Cacosso, J. J. Jacmic, Rate of flow and mechanics of bubble formation from single submerged orifices II: Mechanics of bubble formation, *AIChE Journal* 2 (1956) 300–306.
- [36] S. A. Klotz, Surface-active properties of candida albicans, *Applied and Environmental Microbiology* 55 (1989) 2119–2122.
- [37] F. Zuiderweg, Sieve trays: A view on the state of the art, *Chemical Engineering Science* 37 (1982) 1441 – 1464.
- [38] S. R. Syeda, A. Afacan, K. T. Chuang, A fundamental model for prediction of sieve tray efficiency, *Chemical Engineering Research and Design* 85 (2007) 269 – 277.

- [39] T. M. J. Fabritius, P. T. Kurkinen, P. T. Mure, J. J. Harkki, Vibration of argon-oxygen decarburisation vessel during gas injection, *Ironmaking & Steelmaking* 32 (2005) 113–119.
- [40] R. W. Gross, J. M. Kuhlman, Three-component velocity measurements in a turbulent recirculating bubble-driven liquid flow, *International Journal of Multiphase Flow* 18 (1992) 413 – 421.

Appendix: Shallow Column Flow Regimes

A full discussion of shallow column flow regimes is given in [31], but the following summary here is necessary to support the present analysis. Generally, the character of the multiphase flow in a shallow bubble column depends on the column geometry, superficial velocity, and fluid properties. In the column used in this work with air and water, the dependence of the flow regime on gas superficial velocity and column depth can be defined by a regime map, Fig. 11. The map was constructed by testing a 10×10 grid of depths and superficial velocities in the experimental column without the probe installed. Figure 11 shows that the bubbling of air into water in the test column can be divided into splashing, sloshing, and swirling flow regimes. Unlike regime maps for multiphase flow in tall columns or long tubes, which mainly describe the behavior of the gas phase, these shallow column flow regimes describe the bulk motion of the liquid. The map was constructed using a single column cross-section, so the regime transitions identified in Fig. 11 do not necessarily apply to all shallow columns. However, it is clear from this study that the typical tall-column regime map [26] cannot predict the flow regimes that occur in shallow columns.

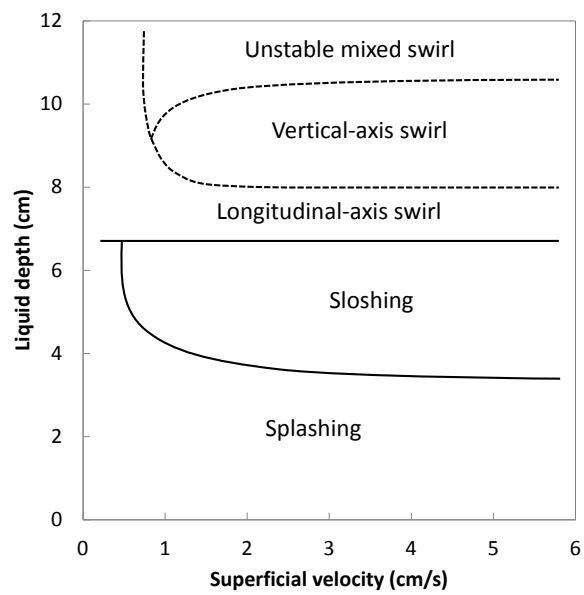


Figure 11: Regime map for the experimental column geometry showing dependence on liquid depth and superficial velocity

When the liquid is very shallow (less than around 4 cm deep), only splashing is observed. This regime is similar to the spray regime noted by Zuiderweg [37] and the froth regime described by Syeda et al. [38] in sieve trays. Liquid filaments, some of which break into drops, extend out of the liquid.

Sloshing, characterized by spontaneous and sustained back-and-forth motion of the liquid, was observed in columns of 4-6 cm depth. The phenomenon of sloshing caused by gas injection has been previously noted in the blowing of gas through molten stainless steel during argon-oxygen decarburization [39]. In the experimental column, the dominant sloshing mode was across the shorter length of the rectangular tank at approximately 2 Hz.

The swirl regime, which occurred when the liquid was deeper, encompasses swirling flow around several axes. The regime map, Fig. 11, shows how the swirl type evolves as the liquid depth is increased. Swirl directions are illustrated and photographed in [31]. Vertical-axis swirl was observed to turn in either direction, which suggests that it was not due to an imbalance in the sparger. Above a depth of 10 cm, the flow begins to switch spontaneously (and seemingly chaotically) between longitudinal, circumferential, and both directions of vertical swirl. Circumferential-axis swirl is common in tall columns [34], but vertical-axis swirl is not [40]. Longitudinal-axis swirl is a natural variation of circumferential-axis swirl for a rectangular column.